Supplementary Information

Three-Dimensional Hollow Sphere of Tetragonal-Spinel $MgMn_2O_4$ Cathode for High-Performance Magnesium Ion Batteries

Shi Tao,[*a] Weifeng Huang,[b] Yushen Liu,[a] Shuangming Chen,[c] Bin Qian,[a] Li Song,[*c]

[a] Department of Physics and Electronic Engineering, Jiangsu Laboratory of Advanced Functional Materials, Changshu Institute of Technology, Changshu 215500, People's Republic of China. *E-mail address: taoshi@cslg.edu.cn(S.Tao)

[b] College of Engineering, Peking University, 100871, People's Republic of China. *E-mail address: hwf@pku.edu.cn (W. Huang)

[c] National Synchrotron Radiation Laboratory, University of Science and Technology of China, Hefei, Anhui 230026, People's Republic of China. *E-mail address: song2012@ustc.edu.cn(L .Song)

Experimental Section

Synthesis of T-$MgMn_2O_4$: In a typical synthesis, 0.3 mmol of $Mg(Ac)_2$ and 0.6 mmol of $Mn(Ac)_2$ were mixed into 50ml ethylene glycol (EG) to form a transparent pink solution, and then 100mg polyvinylpyrrolidone was added into above solution. Taking the above solution heated to 170 °C under magnetic stirring, then keep stirring 2h under refluxing condition. After finished the heating process, cooling it to room temperature, the dark pink solution was washed three times with ethanol, and dried at 80 °C in a vacuum oven overnight. The as-synthesized MgMn-precursor was then heated to 550 °C at the rate of 1 °C min^{-1}, and kept it 2 hours with air condition.

Materials characterization: the X-ray diffraction feature pattern was carried out on the Bruker D-8 advance diffractometer equipped with a Cu Ka radiation (=1.5406 Å). And the data analyzed for GASA Rietveld refinement was scanned over a 2 range

from 10 to 120 degree at a step of 0.02 degree for 8s. The other X-ray diffraction patterns were scanned from 10 to 80 degree at a step of 0.02 degree for 0.5s. The morphology of the samples was recorded by Scanning electron microscopy (SEM) (JEOL-4800) and transmission electron microscopy (TEM) (JEM-2100F). The chemical composition and elemental mapping were analyzed by energy dispersion spectroscopy (EDS) mapping techniques depending on JEOL-4800 with Bruker X-ray sources. The high revolution TEM images were recorded by JEM-2100F. The thermal stability of the samples was evaluated at a heating rate of 2 ℃ min^{-1} from room temperature to 700 ℃ in air using thermo-gravimetric analyzer. The soft X-ray absorption spectroscopy (SXAS) of Mn at L edges was carried out on the soft X-ray beam line at Beijing synchrotron radiation facility (BSRF). The nitrogen sorption measurement was performed on the Accelerated Surface Area & Porosimetry Sstem-ASAP2020. The XPS experiments were carried out on a PHI-5400 electron spectrometer. Elemental composition was measured via inductively coupled plasma atomic emission spectrometry (ICP-AES) with a Thermo Scientific ICAP ICP-MS.

Electrochemical measurement: the working electrode was prepared by mixing target sample (T-$MgMn_2O_4$) with acetylene black and polyvinylidene fluoride binder (PVDF) with a weight ratio of 8/1/1. After mixed homogeneously in isopropanol, the above mixture was dropped onto the Toray carbon paper (1.0*1.0 cm). The loading weight of the active material is about 2.2 mg cm^{-2}. The electrode was dried at 100 ℃ for 6 h to remove the remaining solvent. The electrochemical tests were conducted on a three electrode model, the platinum served as counter electrode, the Ag/AgCl as

reference electrode, and our candidate samples were used as work electrode. 1 M $MgSO_4$ aqueous solution used as the electrolyte. Cyclic voltammetry (CV) results were measured on a CHI760E electrochemical workstation at the scan rate of 0.5 mV s^{-1} with a voltage widow of -0.8-1.2 V. The LAND Battery Testing system (model CT2001A, Land, China) was used for the galvanostatic charge and discharge measurements.

Theoretical calculations: Density functional theory (DFT) calculation was performed using the plane-wave based Vienna ab initio simulation package (VASP) with the generalized gradient approximation (GGA) and exchange correlation functional parametrized by Perdew-Burke-Eernzerhof (PBE). The U parameter for the transition metal Mn is 4.0 eV while the energy cutoff was set to 600 eV for all computations. A $2 \times 2 \times 1$ supercell was used to calculate the energy barrier and the distance of Mg vacancies was set at about 10 Å. The self-consistent field (SCF) tolerance in our DFT calculation is 1×10^{-6} eV.

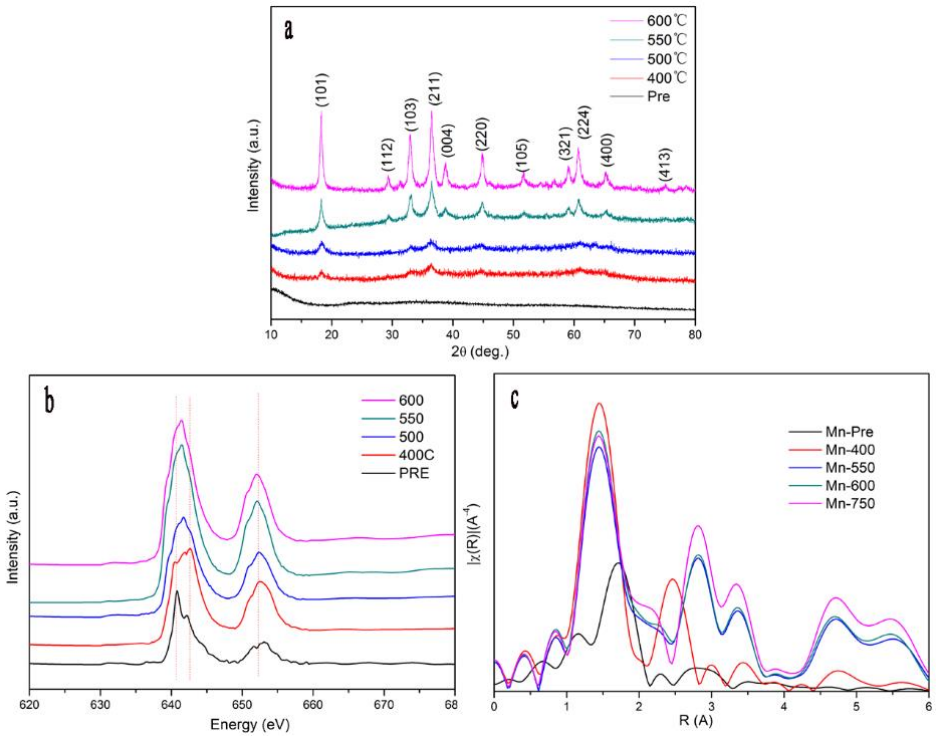

Figure S1. The different samples with different annealing temperatures (a) XRD patterns; (b) the Mn L-edge spectra; (c) Fourier transformation R space for Mn K-edge. The XRD patterns with different annealing temperatures for $MgMn_2O_4$ is shown in figure S1a. It is easily observed the structural evolution from amorphous MgMn-glycerate to crystalline $MgMn_2O_4$.

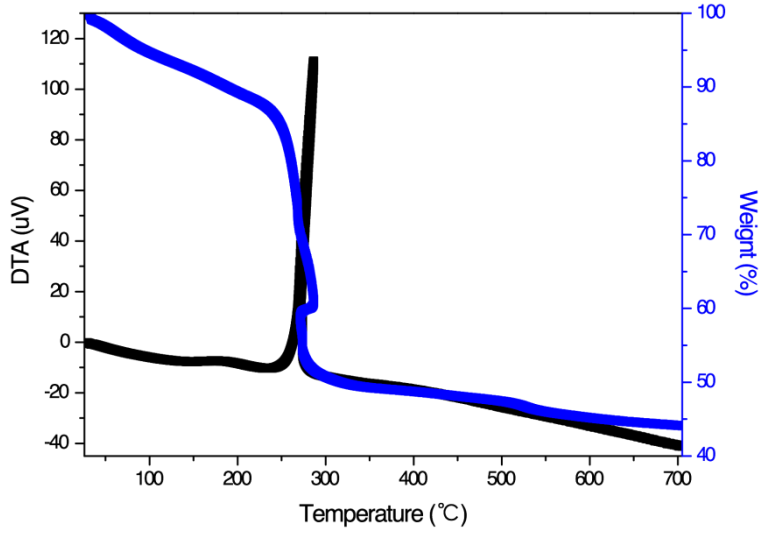

Figure S2. Thermogravimetric analysis (TGA) of MgMn-glycerate precursor spheres at air flow with a temperature ramp of 1 °C min^{-1}.

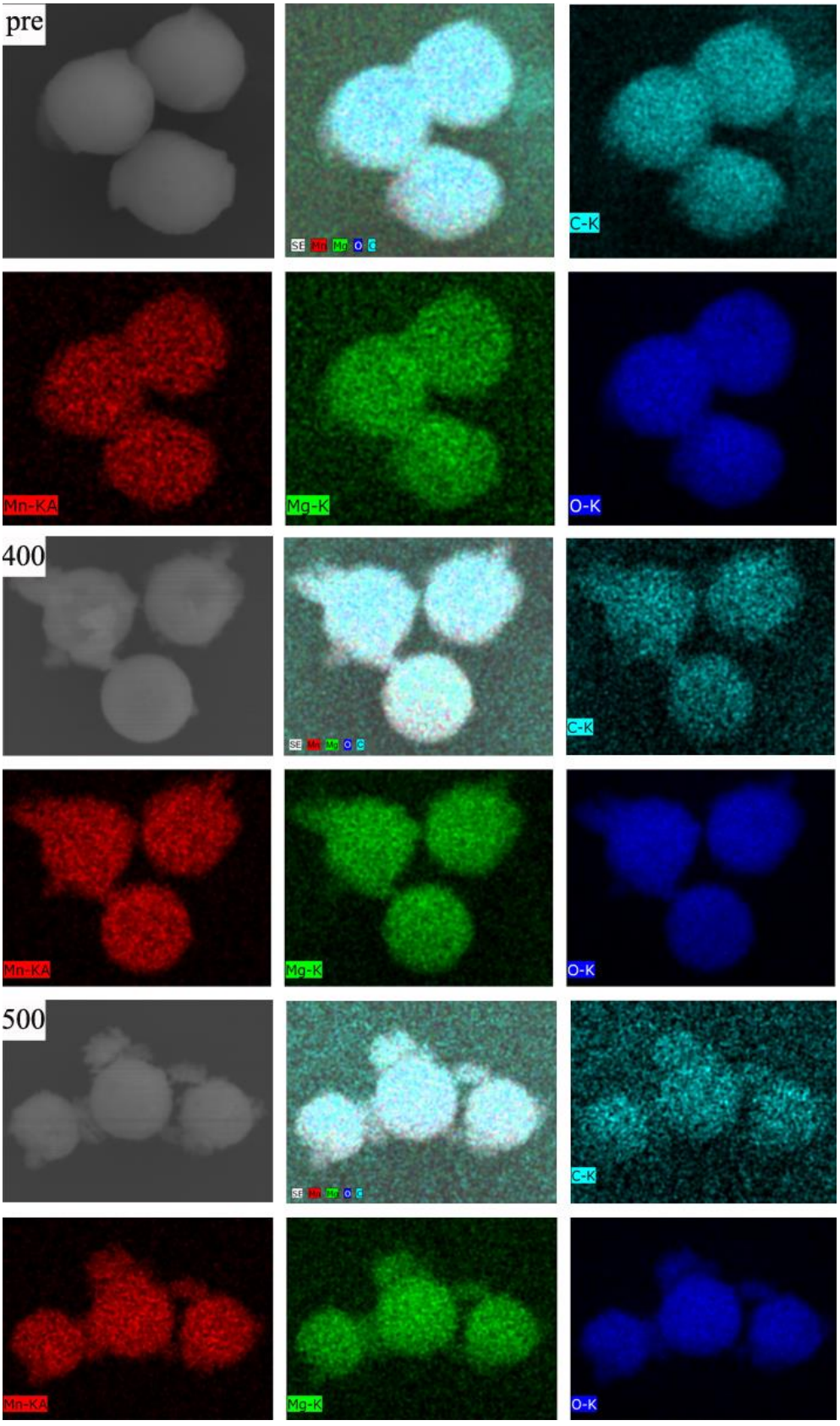

Figure S3. Element mapping for samples with different annealing temperature. The data suggest the uniform distribution of different elements, including C (watchet blue), Mn (red), Mg (green) and O (blue), respectively.

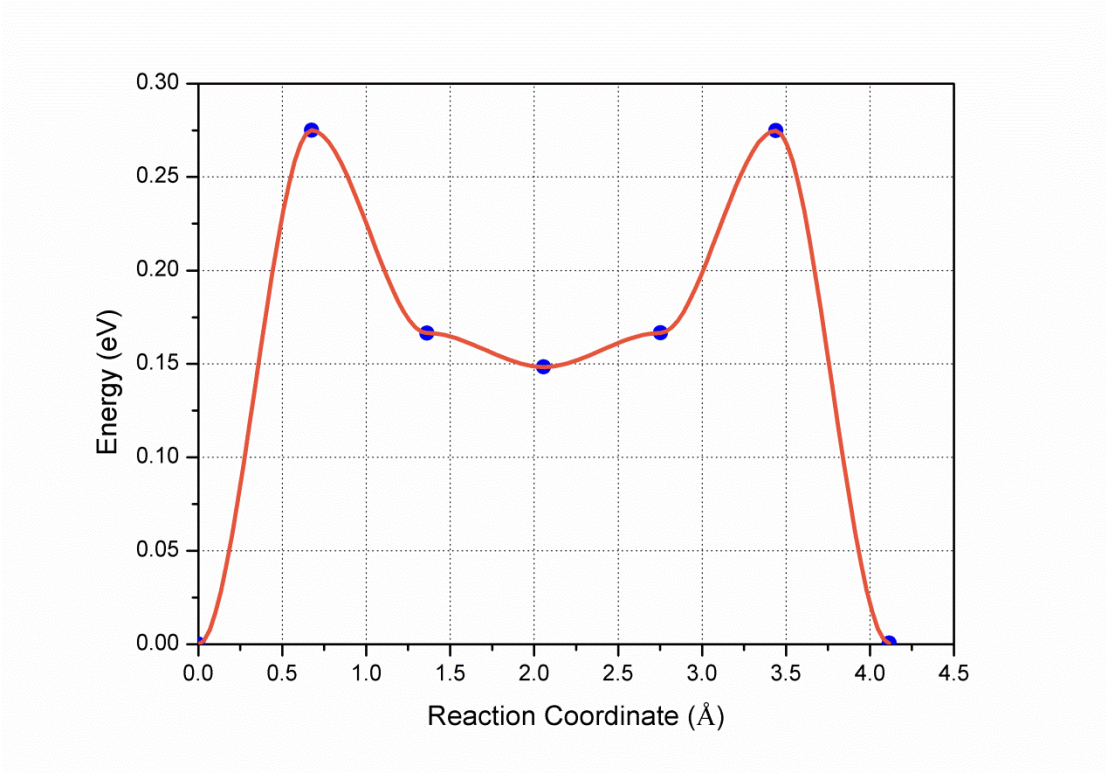

Figure S4. The calculated energy barrier between different Mg^{2+} locations. The low energy barrier at 100 meV suggest an optimized channel for Mg^{2+} ions migration.

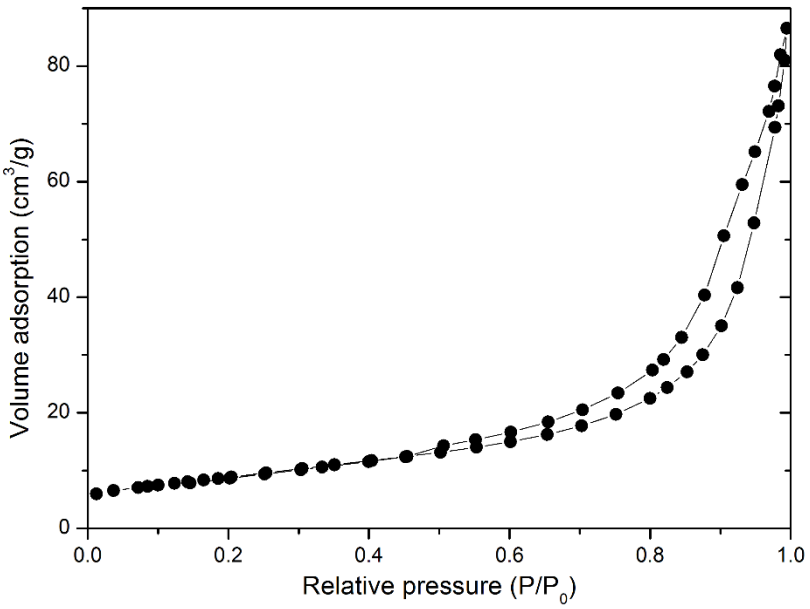

Figure S5. N_2 adsorption/desorption isotherms forT-$MgMn_2O_4$-600.

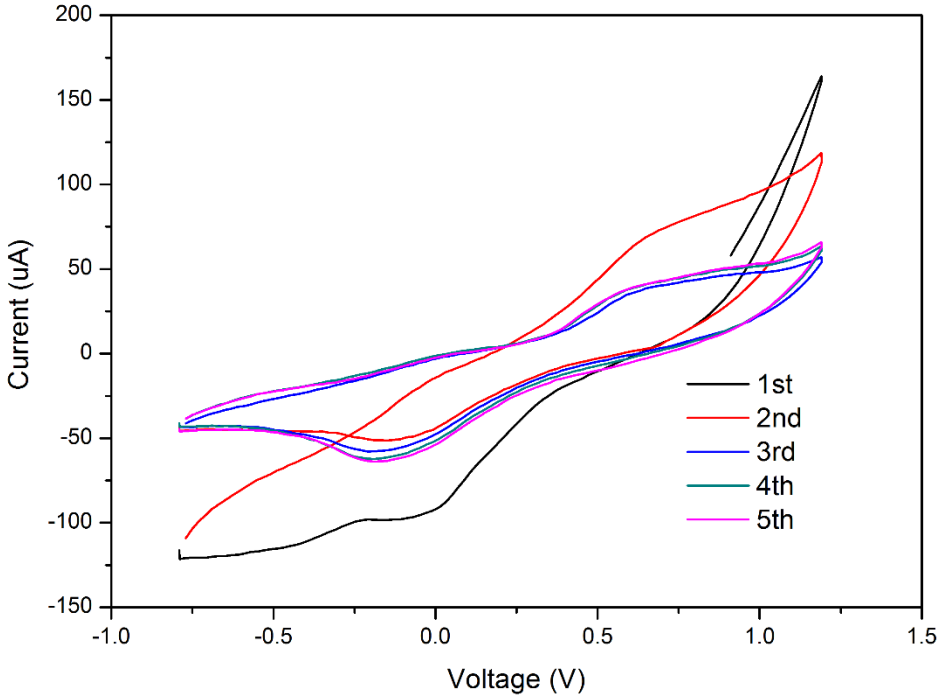

Figure S6. CV curves between -0.8V and 1.2V at a scanning rate of 0.5 mV/s. First four cycles was tested, and it can be observed that the first cycle was different significantly from those following cycles, and no significant variation was observed from the second cycle.

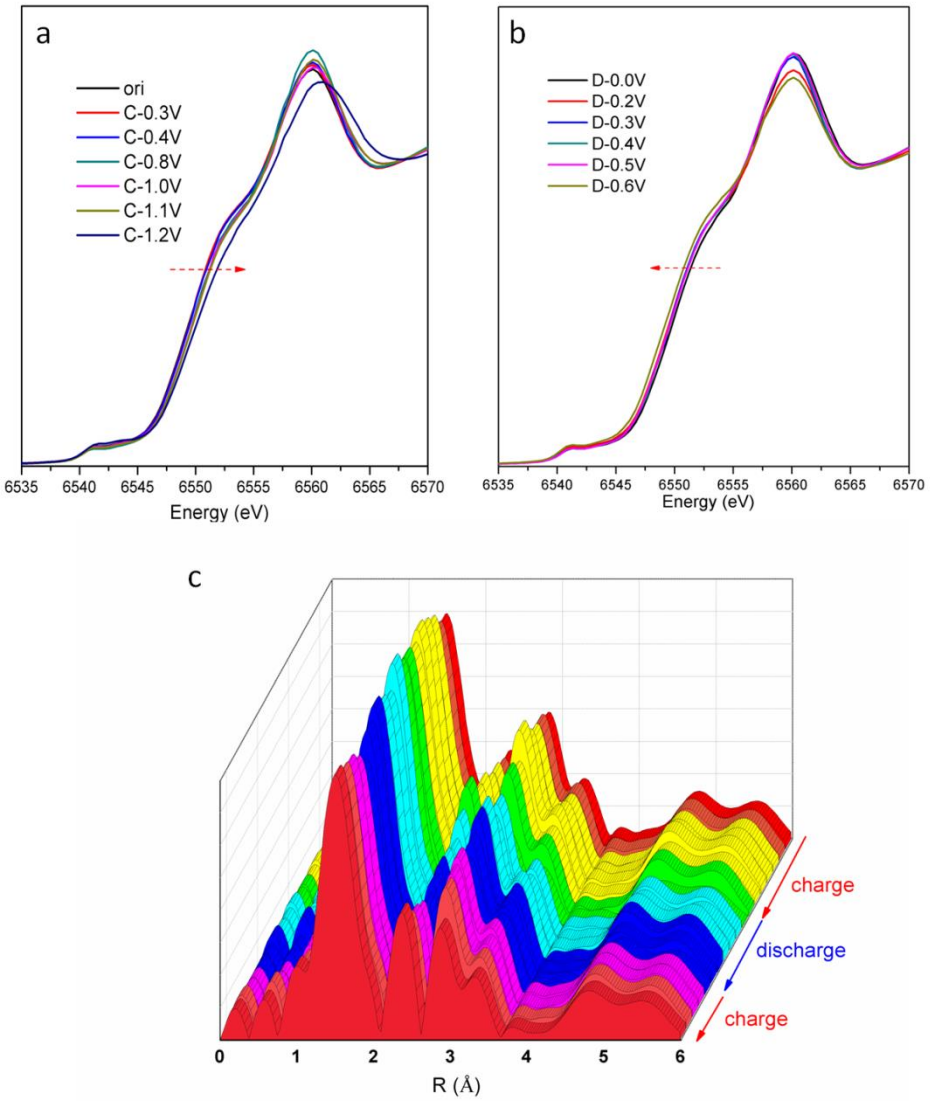

Figure S7. (a) Mn K-edge XANES spectra for different charging potentials. The edge shift points out a clear change to a higher Mn valence state and viceversa in the discharging process (b); (c) Fourier transformation R space at Mn K-edge with different charge/discharge points at the first two cycles. Both of these two structural evolution data suggest that their crystalline structure remains stable during the entire charge/discharge process.

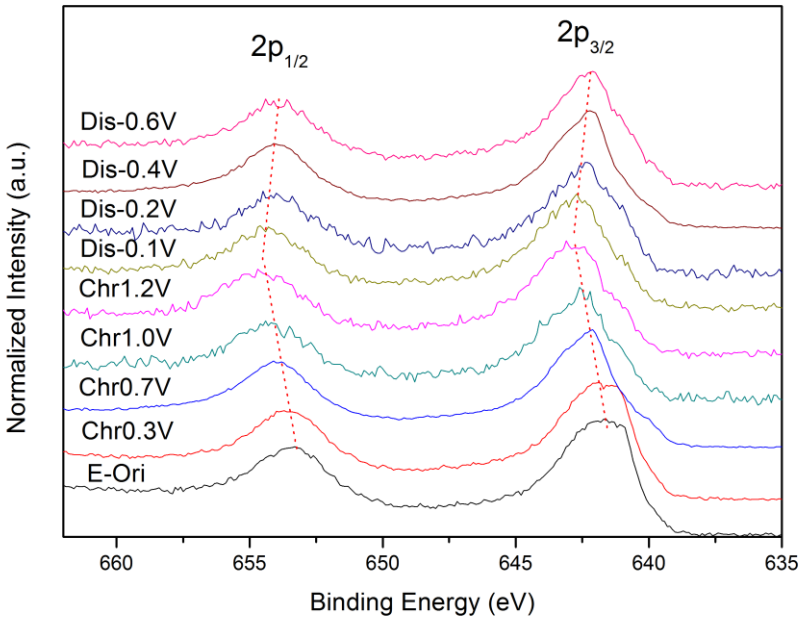

Figure S8. Ex-situ XPS spectra at different charge/discharge states for T-$MgMn_2O_4$.

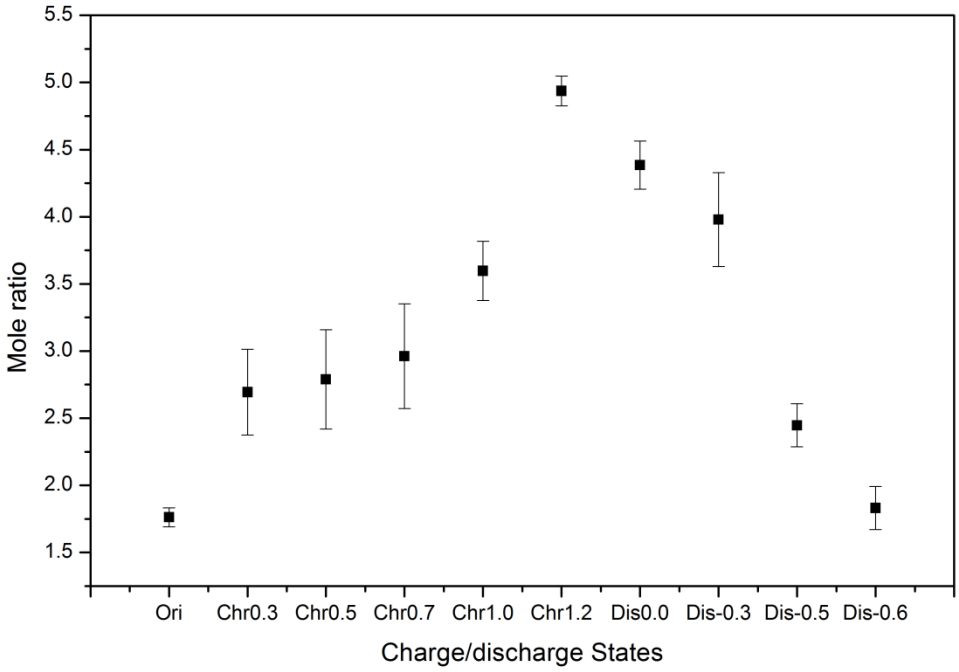

Figure S9. ICP-AES results at different charge/discharge states for T-$MgMn_2O_4$.

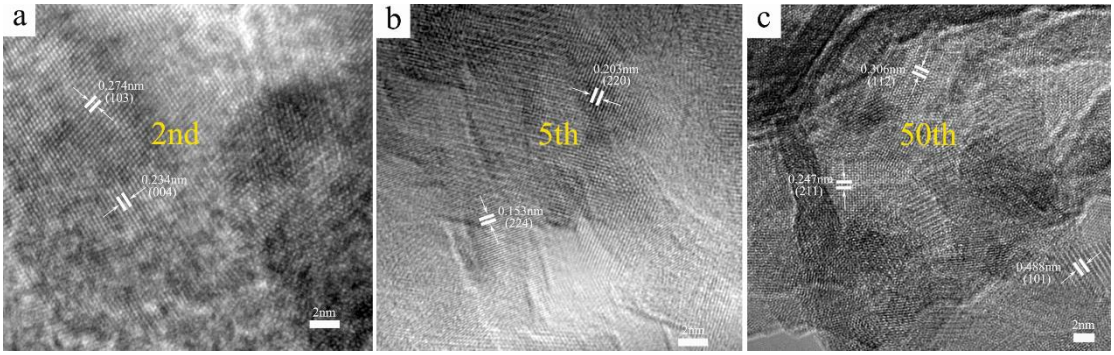

Figure S10. The HRTEM characterization for T-$MgMn_2O_4$ with different cycle numbers. (a) 2 cycles; (b) 5 cycles; (c) 50 cycles. The same crystalline lattice for samples with different cycles indicates the stable structure during the entire electrochemical process.

Table S1. Comparison of the electrochemical performance for $MgMn_2O_4$ in the previous literature with our sample

Electrode materials	Rate perfomance	Cycling performance	Ref
$MgMn_2O_4$	----	85.1 mAh g^{-1} at 60 uA g^{-1} after 20 cycles	1
$MgMn_2O_4$	-----	167 mAh g^{-1} at 4.0 mA g^{-1} after 27 cycles	2
Mg-OMS-1	56.8 mAh g^{-1} at 200 mA g^{-1}	70.8 mAh/g at 100 mA g^{-1} after 300 cycles	3
T-$MgMn_2O_4$	92.6 mAh g^{-1} at 300 mA g^{-1}	260.2 mAh g^{-1} at 100 mA g^{-1} after 300 cycles	This work

References

[1] M. Cabello, R. Alcántara, F. Nacimiento, G. Ortiz, P. Lavela, J. L. Tirado, CrystEngCom. 2015, 17, 8728-8735.

[2] Q. D. Truong, M. K. Devaraju, P. D. Tran, Y. Gambe, K. Nayuki, Y. Sasaki, T. Honma, Chem. Mater. 2017, 29, 6245-6251.

[3] H. Y. Zhang, K. Ye, S. X. Shao, X. Wang, K. Cheng, X. Xiao, G. L. Wang, D. X. Cao, Electrochim. Acta 2017, 229, 371-379.